Available online at www.sciencedirect.com

ScienceDirect

Energy Procedia 142 (2017) 321–327

Energy Procedia

www.elsevier.com/locate/procedia

9th International Conference on Applied Energy, ICAE2017, 21-24 August 2017, Cardiff, UK

A Study on the Wind-Induced Flutter Energy Harvester (WIFEH) Integration into Buildings

Angelo I. Aquino[a,*], John Kaiser Calautit[b], Ben Richard Hughes[a]

[a]*Department of Mechanical Engineering, University of Sheffield, UK*
[b]*Department of Architechture and Built Environment, University of Notthingham, UK*

Abstract

In this modern age, low-energy devices are pervasive especially when considering their applications in the built-environment. This study investigates the potential building integration and energy harnessing capabilities of the Wind-Induced Flutter Energy Harvester (WIFEH) – a microgenerator intended to provide energy for low-powered applications. The work presents the experimental investigation of the WIFEH inside a wind tunnel and a case study using Computational Fluid Dynamics (CFD) modelling of a building integrated with a WIFEH system. The experiments examined the WIFEH under various wind tunnel wind speeds varying between 2.3 up to 10 m/s in order to gauge the induced voltage generation capability of the device. The WIFEH was able to generate an RMS voltage of 3 V, peak-to-peak voltage of 8.72 V and short-circuit current of 1 mA when subjected to airflow of 2.3 m/s. With an increase of wind velocity to 5 m/s and subsequent membrane retensioning, the RMS and peak-to-peak voltages and short-circuit current also increase to 4.88 V, 18.2 V, and 3.75 mA, respectively. The simulation used a gable-roof type building model with a 27˚ pitch obtained from the literature. For the CFD modelling integrating the WIFEH into a building, the apex of the roof of the building yielded the highest power output for the device due to flow speed-up maximisation in this region. This location produced the largest power output under the 45˚ angle of approach, generating an estimated 62.4 mW of power under accelerated wind in device position of up to 6.2 m/s. The method and results presented in this work could be useful for the further investigation of the integration of the WIFEH in the urban environment.

Peer-review under responsibility of the scientific committee of the 9th International Conference on Applied Energy.

Keywords: Airflow; Aeroelastic flutter; Buildings; Computational Fluid Dynamics (CFD); Simulation; Wind; Wind belt

1. Introduction

At the present day, buildings account for 20-40% of total energy consumption in developed countries, an amount greater than consumptions of both industry and transport sectors [1]. A foremost advantage of developing wind energy

1876-6102
Peer-review under responsibility of the scientific committee of the 9th International Conference on Applied Energy.
10.1016/j.egypro.2017.12.051

harvesting in buildings is clear - bringing the power plant closer to the power consumers. Because of the sharing and dissemination of power creation means to the public, higher energy efficiencies can be expected, together with diminished dependence to energy companies, lower carbon footprint and overall stimulation of the economy [2]. Add to the foregoing, distributed power generation will suggestively decrease the load of the grid, dependence on diesel generators (in events of power outage) and power transmission costs.

A novel and emerging alternative to the usual turbines are wind-induced flutter energy harvesters. In this fast-changing world, low-energy power generation devices have been gathering increased attention because of their potential integration with self-powered micro-devices and wireless sensor networks especially in the urban setting. The power produced by these microgenerators is sufficient to run light-emitting diodes, stand-alone wireless sensor nodes and small liquid crystal displays [3]–[5]. Unlike turbine-based generators, the WIFEH is a small-scale, light and economical direct-conversion energy harvester which does not need any gears, rotors or bearings. Wind flowing into and around a tensioned membrane or belt causes the membrane to flutter initiating connected permanent magnets to vibrate relative to a set of coils. This motion induces a current flowing in the coil, thereby generating electric power [6]–[8].

2. Literature review and objectives

One of the incipient technologies with respect to low-energy wind harnessing is the group regarded as “flutter-based” energy harvesters. These devices stand as alternatives to conventional wind turbines and have certain advantages in terms of the absence of component moving parts, leading to reduced production costs and longer system lifespan. Important to note as well that flutter-based wind energy can even be designed to adapt to highly fluctuating wind speeds and changing directions [9].

In order to increase the lifespans of Wireless Sensor Networks (WSN), continuous research is being directed in terms of alternative power sources that are appropriate for their scale. WSN technologies are currently deployed in the milliWatt and microWatt consumption power range [10]. This can be noticed as an attractive and lucrative niche for small-scale energy harvesters, most notably the type we now consider as the WIFEH. This wind energy harvester makes use of aeroelastic flutter to convert the kinetic energy contained in wind into electrical energy.

In this paper, the evaluation of the energy harnessing potential of the WIFEH is discussed. The evaluation is done two-fold: (i) through experimental investigation of the harvester prototype conducted inside a wind tunnel; and (ii) through CFD analysis relating external conditions and harvester location to harvester power generation capabilities. The experimental analysis will assess a constructed WIFEH prototype’s performance when subjected to different wind tunnel airflow velocities. The CFD analysis will investigate the effect of various external conditions and device locations on the performance of the WIFEH. The simulation will use a gable-roof type building model with a 27° pitch [11]. The atmospheric boundary layer (ABL) flow will be used for the simulation of the incident wind.

3. Evaluation of the operation of the WIFEH prototype through wind tunnel tests

To characterise the effect of various wind speeds to the harvester’s performance, a prototype was constructed and tested inside a wind tunnel. The prototype was tested under varying wind tunnel airflow speeds to enable the measurement of RMS voltage, peak-to-peak voltage and short-circuit current generated by the harvester in response to the different wind velocities. A schematic diagram of the WIFEH is shown in Figure 1 a) while the prototype schematic positioning is depicted in Figure 1 b).

The WIFEH prototype with one coil and eight stacked 1.5 mm-thick 10 mm-diameter magnets was tested for preliminary experimental results inside the wind tunnel which is a low-speed closed-loop wind tunnel detailed in [12]. The wind tunnel had a test section with the dimensions of 0.5, 0.5, and 1 m (see Figure 2). The flow in the wind tunnel was characterised prior to experimental testing to indicate the non-uniformity and turbulence intensity in the test-section which was 0.6% and 0.49% and according to the recommended guidelines [12].

For data gathering, the system was connected to a Tektronix TBS1052B Digital Storage Oscilloscope positioned outside the wind tunnel. The wind speed inside the tunnel was varied from the wind tunnel minimum of 2.3 m/s to maxima of (i) 8 m/s without belt retensioning and (ii) 10 m/s with belt retensioning. It should be noted that without

retensioning, the performance of the belt did not improve beyond 8 m/s. Without membrane retensioning there was observed self-sustained but unstable oscillations leading to irregular voltage signal readings.

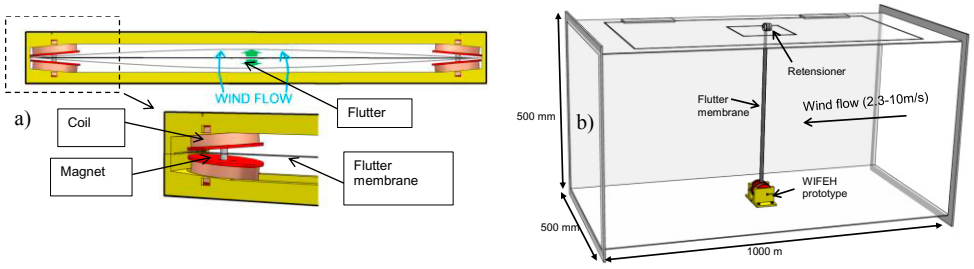

Fig. 1. Schematic diagrams of a) a quad (4-coil arrangement) WIFEH b) a WIFEH prototype inside the wind tunnel test section

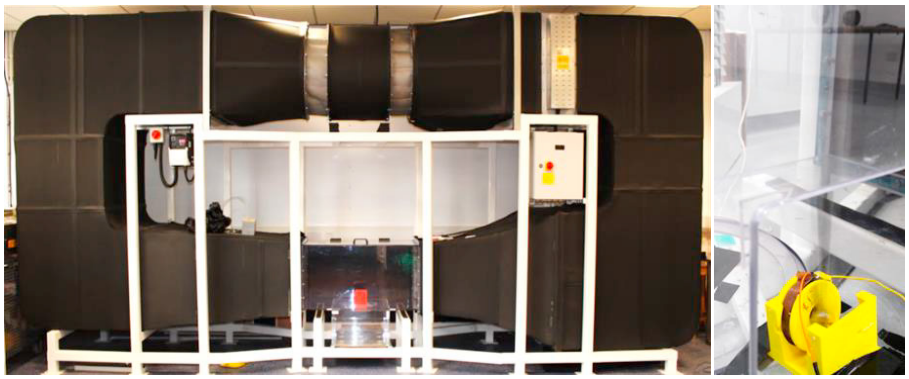

Fig. 2. (a) Side view of the closed-loop wind tunnel (b) WIFEH prototype with one coil configuration showing flutter motion at 2.3 m/s

The voltage waveform pertinent attributes such as the maximum value, peak-to-peak voltage, root-mean-square (RMS) voltage and frequency could be observed instantaneously in the 7-inch WVGA TFT colour display monitor of the oscilloscope. The instrument has 3% vertical (voltage) measurement accuracy permitting the user to see all signal details. Measurements were taken uninterruptedly producing a continuous waveform that is displayed in oscilloscope's LCD monitor and were recorded in a storage device connected to the oscilloscope USB port.

The WIFEH model used for the wind tunnel testing was in part constructed using 3D printing. The copper wire used to make the conducting coil was enamelled copper wire 40 SWG (Standard Wire Gauge) with 0.125 mm diameter. The circular casing was 3D-printed using HP Designjet 3D Printer. The outer diameter of the casing was 54 mm and the inner diameter (hole diameter) was 12.5 mm, with outer thickness of 20 mm and inner spacing for the coil winding of 12 mm. Approximately 2500 turns were looped to produce the coil. The internal resistance of the coil was measured to be 1150 Ohms. For comparison, the coil used in the transducer in the device from S. Frayne was made of 38 AWG enamel coated wire with approximately 150 turns and resistance of approximately 25 ohms [13].

The AC Voltage waveform produced by the WIFEH system when subjected to a constant airflow of 2.3 m/s is shown in Figure 3 a), which was forming a regular pattern of sinusoidal wave. This first trial corresponds to the initial and minimum flow velocity of the wind tunnel. The RMS voltage was measured to be 3.00 V. The RMS voltage is the effective value of a varying voltage source such as the WIFEH. The maximum voltage reading was 3.84 V while the peak-to-peak voltage was 8.72 V.

Without prior retensioning the membrane, the wind tunnel airflow speed was increased to 5 m/s and the AC voltage signal was again observed and recorded as shown in Figure 3 b). The waveform is not as regular as for the previous case and we can observe more occurrences of sharper turns with resemblance to sawtooth signals, with decreasing magnitude of the negative peaks of the signal. The recorded RMS for 5 m/s wind speed is 4.16 V with peak-to-peak value 18.4 V and maximum value of 8.8 V.

The membrane of the WIFEH was then retensioned while maintaining the wind tunnel airflow speed of 5 m/s. The AC Voltage waveform produced by the harvester system when subjected to a constant airflow was again recorded. A regular pattern of sinusoidal wave with minor and major peaks was again observed. Under this wind condition, the microgenerator generated an RMS voltage of 4.88 V with maximum of 9.20 V and peak-to-peak value of 18.2 V. This is shown in Figure 4 a).

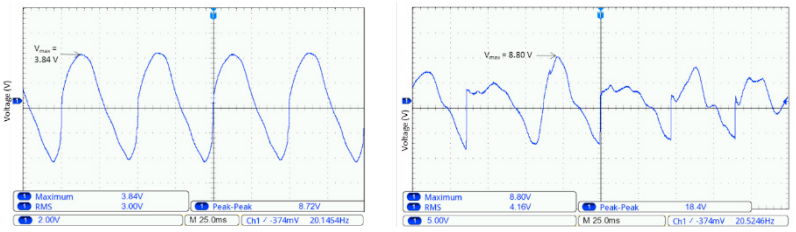

Fig. 3 a) Open-circuit voltage of the Wind-Induced Flutter Energy Harvester (WIFEH) without membrane retensioning a) under 2.3 m/s flow velocity b) under 5 m/s flow velocity

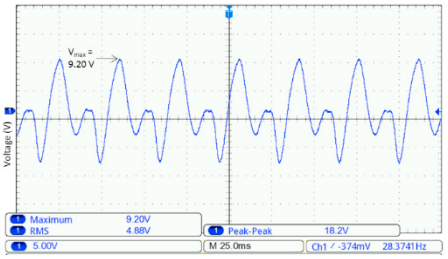

Fig. 4 Open-circuit voltage of the Wind-Induced Flutter Energy Harvester (WIFEH) with membrane retensioning under 5 m/s flow velocity

Incremental increases of 1 m/s airflow speed was also directed for two cases: (i) without belt retensioning and (ii) with belt retensioning, starting from 2.3 m/s. The open-circuit voltage and short-circuit current were then observed using a digital multimeter after each incremental rise. It can be remarked that for the case without belt retensioning the maximum open-circuit voltage and short-circuit current both occurred for 6 m/s airflow speed, beyond which there was a significant drop in both variables. This was due to the observation that beyond said airflow speed the belt started to perform less stable oscillations compared to cases of lower wind speeds. This unstable flutter greatly influences the magnets-coil relative dynamic positioning, therefore affecting the induced voltage and current in the conducting coil. Thus the relationship between airflow speed and open-circuit voltage or short-circuit current was not observed to be linear (see Figure 5). However, with retensioning of the belt the linear relationship between airflow and voltage / current resume. The trend continued even up to 10 m/s airflow speed.

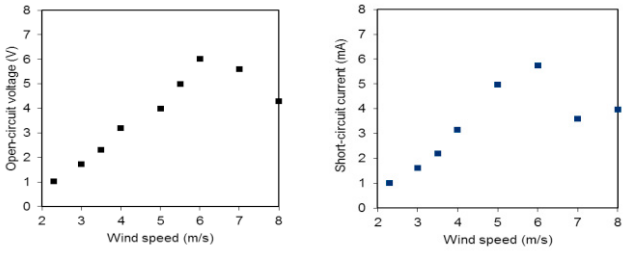

Fig. 5 Electrical output performance of the WIFEH without retensioning under various flow velocities: (a) Open-circuit voltage (b) Short-circuit current

4. Computational Fluid Dynamics (CFD) analysis of WIFEH integration into buildings

The system of the WIFEH integrated into a building was modelled using CFD through ANSYS Fluent simulating the airflow pattern, velocity magnitude and distribution around the building and within and surrounding the energy harvester. This was performed to allow for optimisation of the positioning of the energy harvester throughout the

various building sections. This investigation simulated a gentle breeze, which is category 3 in the Beaufort wind force scale. The flow was modelled by using the standard k–ϵ turbulence model, which is a well-established method in research on wind flows around buildings [11], [14]–[16].

Figure 6 a) shows the velocity contours of a side view cross-sectional plane inside the computational domain representing the airflow distribution around the building integrated with WIFEH. The left hand side of the plot shows the scale of airflow velocity in m/s. The contour plot in the fluid domain is colour coded and related to the CFD colour map, ranging from 0 to 5.9 m/s. As observed, the approach wind profile entered from the right side of the domain and the airflow slowed down as it approached the building and lifted up. Zoomed in views of the velocity distribution around the WIFEH devices R1, R2 and R3 are shown on top of the diagram. The results showed that the shape and angle of the roof had a significant impact on the performance of the WIFEH. In the diagram, it is clear that locating the device at the leeward side of the roof will result in little to no energy generation due to the low wind speeds in this area. However, it should be noted that this was not the case for other wind angles, for example when the wind is from the opposite direction. Therefore, location surveying, wind assessment and detailed modelling are very important when installing devices in buildings. At wind velocity (U_H) 4.7 m/s and 0° wind direction, the airflow speed in R1 was the highest at 4.5m/s while the lowest was observed for the R2 WIFEH located at the centre of the roof.

Figure 6 b) displays the velocity contours of a top view cross-sectional plane inside the computational domain representing the airflow distribution around the building integrated with WIFEH. The approach wind profile entered from the right side of the domain and the airflow slowed down as it approached the building and accelerated as it flowed around the corners. Zoomed in views of the velocity distribution around the WIFEH devices F1-F3 and S1-S3 are shown on top and right side of the diagram. At wind velocity (U_H) 4.7 m/s and 0° wind direction, the airflow speed in F1 and F3 were the highest at 5.4m/s while the lowest was observed for the S2 and F2 WIFEH located at the airflow recirculation zones. Figure 7 compares the estimated output of the device located in the three locations F3, S3 and R3 at various outdoor wind speeds. Among these three locations, at 30° wind direction, R3 provided the highest output ranging between 2.5 to 15.2 V, while F3 showed the lowest output.

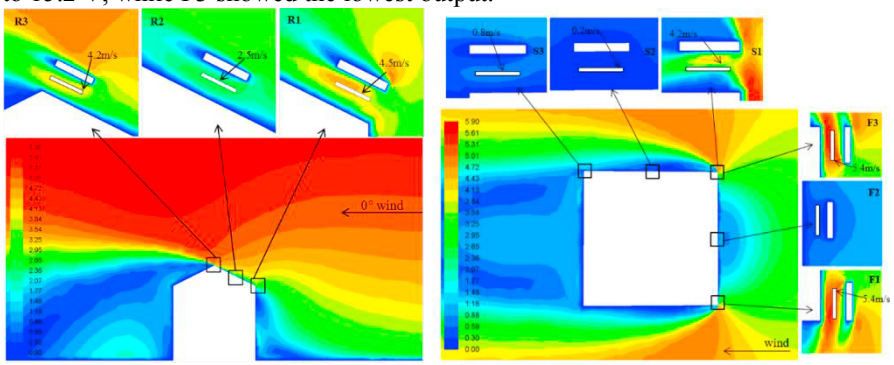

Fig. 6. a) Contours of velocity magnitude showing a) cross-sectional side view of the building b) cross-sectional top view of the building

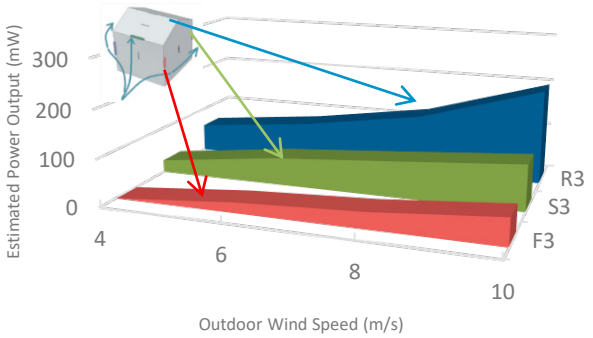

Fig. 7. Impact of various outdoor wind speeds (U_H) on the estimated output of the WIFEH for locations F3, S3 and R3

5. Conclusions

The Wind-Induced Flutter Energy Harvester is valuable for low-energy wind harvesting in the built environment due to its low cost and modularity. With increasing airflow speed came increases in open-circuit voltage and short-circuit current produced by the WIFEH. Regular sinusoidal waveform voltage signals were observed through a digital oscilloscope for wind tunnel airflow speeds of 2.3 m/s and 5 m/s with the belt retensioned. The waveform pattern became less regular for 5 m/s airflow without belt retensioning. The RMS (effective) voltages recorded were 3.0 V and 4.88 V with maximum values of 3.84 V and 9.20 V for 2.3 m/s and 5 m/s wind tunnel airflow speeds, respectively.

With respect to the simulations for WIFEH building locations, the apex of the roof of the building provided the greatest power yield, with this location's production being the largest with the 45-degree approach of the wind relative to the building. Optimum installation of the WIFEH devices therefore translates to prioritising the roof and the trailing edges of the building to yield the highest possible power generation, depending on wind conditions, not the leading edge nor centres of surfaces.

The possibility of assembling an array of WIFEHs can create the potential for further scaling up of the system. The results stated the significance of using detailed CFD analysis to evaluate the device and its surroundings. The detailed velocity distribution results showed the capabilities of CFD on evaluating the optimum positioning of the devices around the building. The modelling procedure and data presented in this work can be used by engineers and researchers to further investigate the integration of the WIFEH in the urban environment.

Acknowledgment

We would like to thank British Council (DOST-Newton Fund no.209559487) for the funding of this research.

References

[1] Pérez-Lombard, L., Ortiz, J., and Pout, C., "A review on buildings energy consumption information," *Energy and Buildings*, vol. 40, no. 3, pp. 394–398, 2008.

[2] Toja-Silva, F., Lopez-Garcia, O., Peralta, C., Navarro, J., and Cruz, I., "An empirical-heuristic optimization of the building-roof geometry for urban wind energy exploitation on high-rise buildings," *Applied Energy*, vol. 164, pp. 769–794, 2016.

[3] Hu, Y., Zhang, Y., Xu, C., Lin, L., Snyder, R. L., and Wang, Z. L., "Self-powered system with wireless data transmission," *Nano Letters*, vol. 11, no. 6, pp. 2572–2577, Jun. 2011.

[4] Zhu, G., Yang, R., Wang, S., and Wang, Z., "Flexible high-output nanogenerator based on lateral ZnO nanowire array," *Nano Letters*, vol. 10, no. 8, pp. 3151–3155, 2010.

[5] Hu, Y., Zhang, Y., Xu, C., Zhu, G., and Wang, Z., "High-output nanogenerator by rational unipolar assembly of conical nanowires and its application for driving a small liquid crystal display," *Nano Letters*, vol. 10, no. 12, pp. 5025–5031, 2010.

[6] Aquino, A. I., Calautit, J. K., and Hughes, B. R., "Integration of aero-elastic belt into the built environment for low-energy wind harnessing," no. 209559487, p. 10.

[7] Aquino, A. I., Calautit, J. K., and Hughes, B. R., "Urban Integration of Aeroelastic Belt for Low-Energy Wind Harvesting," *Energy Procedia*, vol. 105, pp. 738–743, 2017.

[8] Aquino, A. I., Calautit, J. K., and Hughes, B. R., "Evaluation of the Integration of the Wind-Induced Flutter Energy Harvester (WIFEH) into the Built Environment : Experimental and Numerical Analysis," pp. 1–21.

[9] Arroyo, E., Foong, S., and Maréchal, L., "Experimental study of an omni-directional wind fluttering energy harvester," in *ASME 2014 Dynamic Systems and Control Conference*, 2014, p. V003T53A002-V003T53A002.

[10] Ramasur, D. and Hancke, G. P., "A wind energy harvester for low power wireless sensor networks," *Instrumentation and Measurement Technology Conference (I2MTC), 2012 IEEE International*, pp. 2623–2627, 2012.

[11] Tominaga, Y., Akabayashi, S., Kitahara, T., and Arinami, Y., "Air flow around isolated gable-roof buildings with different roof pitches: Wind tunnel experiments and CFD simulations," *Building and Environment*, vol. 84, pp. 204–213, 2015.

[12] Calautit, J. K., Chaudhry, H. N., Hughes, B. R., and Sim, L. F., "A validated design methodology for a closed-loop subsonic wind tunnel," *Journal of Wind Engineering and Industrial Aerodynamics*, vol. 125, pp. 180–194, 2014.

[13] Frayne, S. M., "(12) Ulllted States Patent (45) Date of Patent :," vol. 2, no. 12, 2009.

[14] Sofotasiou, P., Calautit, J. K., Hughes, B. R., and O'Connor, D., "Towards an integrated computational method to determine internal

spaces for optimum environmental conditions," *Computers & Fluids*, vol. 127, pp. 146–160, 2016.

[15] Shahzad, S., Calautit, J. K., Aquino, A. I., Nasir, D. S. N. M., and Hughes, B. R., "A user-controlled thermal chair for an open plan workplace: CFD and field studies of thermal comfort performance," *Applied Energy*, 2017.

[16] Kaiser, J., Aquino, A. I., Shahzad, S., Snm, D., and Richard, B., "Thermal comfort and indoor air quality analysis of a low- energy cooling windcatcher," vol. 0, pp. 3–8, 2016.